UNIVERSITY OF BIRMINGHAM

Research at Birmingham

Design and characterisation of a new duplex surface system based on S-phase hardening and carbon-based coating for ASTM F1537 Co–Cr–Mo alloy

Luo, Xia; Li, Xiaoying

DOI:
10.1016/j.apsusc.2013.11.141

License:
Creative Commons: Attribution-NonCommercial-NoDerivs (CC BY-NC-ND)

Document Version
Publisher's PDF, also known as Version of record

Citation for published version (Harvard):
Luo, X & Li, X-Y 2014, 'Design and characterisation of a new duplex surface system based on S-phase hardening and carbon-based coating for ASTM F1537 Co–Cr–Mo alloy', Applied Surface Science, vol. 292, pp. 336-344. https://doi.org/10.1016/j.apsusc.2013.11.141

Link to publication on Research at Birmingham portal

Publisher Rights Statement:
Eligibility for repository : checked 03/04/2014

General rights
Unless a licence is specified above, all rights (including copyright and moral rights) in this document are retained by the authors and/or the copyright holders. The express permission of the copyright holder must be obtained for any use of this material other than for purposes permitted by law.

• Users may freely distribute the URL that is used to identify this publication.
• Users may download and/or print one copy of the publication from the University of Birmingham research portal for the purpose of private study or non-commercial research.
• User may use extracts from the document in line with the concept of 'fair dealing' under the Copyright, Designs and Patents Act 1988 (?)
• Users may not further distribute the material nor use it for the purposes of commercial gain.

Where a licence is displayed above, please note the terms and conditions of the licence govern your use of this document.

When citing, please reference the published version.

Take down policy
While the University of Birmingham exercises care and attention in making items available there are rare occasions when an item has been uploaded in error or has been deemed to be commercially or otherwise sensitive.

If you believe that this is the case for this document, please contact UBIRA@lists.bham.ac.uk providing details and we will remove access to the work immediately and investigate.

Download date: 01. Feb. 2019

Applied Surface Science 292 (2014) 336–344

Contents lists available at ScienceDirect

Applied Surface Science

journal homepage: www.elsevier.com/locate/apsusc

Design and characterisation of a new duplex surface system based on S-phase hardening and carbon-based coating for ASTM F1537 Co–Cr–Mo alloy☆

Xia Luo, Xiaoying Li*

School of Metallurgy and Materials, The University of Birmingham, Edgbaston, Birmingham B15 2TT, UK

ARTICLE INFO

Article history:
Received 5 August 2013
Received in revised form 17 October 2013
Accepted 25 November 2013
Available online 4 December 2013

Keywords:
Co–Cr–Mo alloy
S-phase
GiC coating and duplex surface

ABSTRACT

Co–Cr–Mo alloys are one of the most widely used metallic biomaterials for metal-on-metal joint prostheses. However, concerns over increased revision rates mainly due to nano-sized wear debris have been raised. This study was aimed at enhancing the friction, wear and load-bearing properties of Co–Cr–Mo alloys by developing a new duplex surface system combining super hard and wear-resistant S-phase layer with self-lubricating, low-friction carbon-based coating. To this end, ASTM F1537 Co–Cr–Mo alloy surface was plasma carburised (PC) at 450 °C and then coated with a carbon-based GiC coating. The microstructures of the duplex and single treated (PC or GiC coating) Co–Cr–Mo surface systems were characterized and their mechanical, tribological and corrosion properties were evaluated. The results showed that the new duplex surface system exhibited a high load bearing capacity, a low friction coefficient, excellent wear resistance and good corrosion behaviour.

© 2013 The Authors. Published by Elsevier B.V. All rights reserved.

1. Introduction

Co–Cr–Mo alloys are one of the most widely used metallic biomaterials for metal-on-metal joint prostheses owing to their good mechanical properties, high wear and corrosion resistance and adequate biocompatibility [1]. However, concerns over increased revision rates mainly due to nano-sized wear debris associated with some types of large head metal-on-metal replacements have been raised [2].

Several attempts have been made to extend the life-span of Co–Cr–Mo prosthetic bearing surfaces by means of surface engineering including surface modification and surface coatings. Recently, a super hard carbon super-saturated solid solution, named as S-phase [3], has been successfully produced on the surface of Co–Cr–Mo alloy with an expanded face-centred cubic structure by low temperature plasma carburising [4,5]. The wear resistance of Co–Cr–Mo alloys can be significantly improved by S-phase without loss of corrosion resistance. However, S-phase normally exhibits high friction [6], which is similar to or slightly higher than that of untreated Co–Cr–Mo alloys. High friction can cause large friction moment on joints, thus leading to fretting wear at the joint/bone surface and pre-mature failure; friction-induced temperature rise in physiological loading environment can cause thermal damage in tissue around replacement and decrease of lubrication of synovial fluid [7].

Another potential surface engineering approach to increase the tribological behaviour of Co–Cr–Mo surfaces is to usecarbon-based amorphous coating with a combination of low friction, high wear resistance, chemical inertness and desirable biocompatibility [8–12]. However, the clinic application of carbon-based amorphous coatings for Co–Cr–Mo prosthetic bearing surfaces has been impeded mainly by their unpredictable spallation under physiological loading environment [13,14]. Although the mechanisms involved are still under investigation, two factors are believed to be responsible for the observed spallation of carbon-based amorphous coatings. First, carbon-based amorphous coatings are normally thin (2–3 μm) in order to avoid a high level of residual compressive stress. Therefore, their load bearing capacity is low especially on a relative soft substrate [15] due to the so-called 'thin-ice effect' when the substrate plastically deforms under a high contact stress. Second, like most thin coatings, there are always some pinholes in carbon-based coatings. Galvanic corrosion can occur at the interface between coating and substrate when biological fluids penetrate through these pinholes under a high hydrolic pressure into the interface during the movement of joint replacement [8,13,16].

It could be a promising approach to achieve low-friction, high wear resistance and high load bearing capacity by combining low-friction carbon-based coatings with hard and strong S-phase cases.

☆ This is an open-access article distributed under the terms of the Creative Commons Attribution-NonCommercial-No Derivative Works License, which permits non-commercial use, distribution, and reproduction in any medium, provided the original author and source are credited.

* Corresponding author. Tel.: +44 1214147105.
E-mail addresses: x.li.1@bham.ac.uk, donglixy@gmail.com (X. Li).

0169-4332/$ – see front matter © 2013 The Authors. Published by Elsevier B.V. All rights reserved.
http://dx.doi.org/10.1016/j.apsusc.2013.11.141

Table 1
Chemical composition of as-received materials.

Element	C	Mn	Si	Cr	Mo	N	Co
wt%	0.25	0.76	0.72	28.35	6.9	0.15	Bal.

Hence, the present study was directed at designing a new duplex surface system for ASTM F1537 Co–Cr–Mo alloy by combining a low-temperature carbon diffusion induced hard S-phase layer with a low-friction carbon-based amorphous coating. Systematic characterisation was conducted to study microstructure and evaluate the performance of the new duplex system developed from this study.

2. Experimental

2.1. Material and surface treatments

ASTM F1537 alloy with a nominal composition of Co–28Cr–10Mo was used as the substrate material in this research. The measured chemical composition of the as-received Co–28Cr–10Mo material is listed in Table 1. Samples were cut from 28 mm diameter bar to 6 mm thickness discs. Prior to surface treatments, disc samples were wet ground and polished to a surface finish of R_a = 13.2 nm.

Low-temperature plasma carburising was carried out in a DC plasma unit using the optimal conditions identified by previous research [4]. Prior to the treatment, all the samples were thoroughly cleaned using an ultrasonic cleaner in washing-up liquid and acetone. The samples were plasma carburised at 450 °C for10 h with a gas mixture of H_2 (98.5 vol%) and CH_4 (1.5 vol%). A commercial Cr doped carbon-based Graphit-iC (GiC) coating was deposited by a closed field unbalanced magnetron sputtering system. Two chromium and two carbon targets were used for deposition. The schematic diagram of the deposition system is shown in Fig. 1 [17]. The targets were applied to a DC power, while the substrate was biased with pulsed DC. The deposition procedure consisted of a 20 min of plasma ion cleaning on the chromium target and substrate samples under Ar atmosphere, followed by the deposition of a chromium adhesive layer and then the deposition of Cr/C ramp layer through rotating samples in front of each target. For clarity,

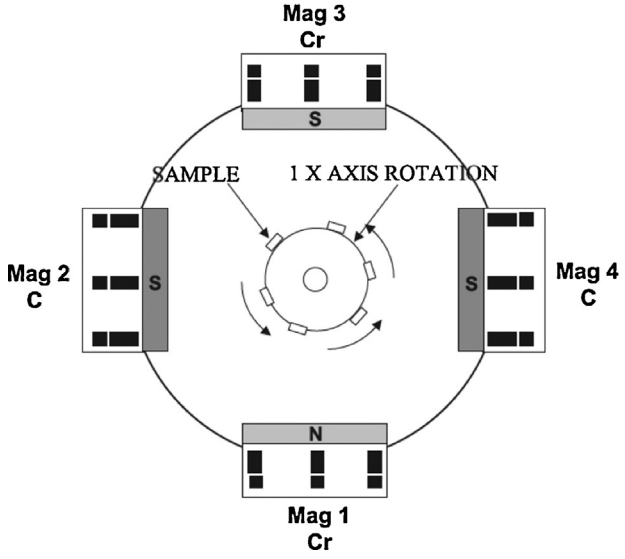

Fig. 1. Schematic diagram of the closed field unbalanced magnetron sputtering system.

Table 2
Sample's codes and conditions.

Code	Sample condition
AR	As-received
PC	Plasma carburised
GiC-AR	GiC coating deposited
GiC-PC	Plasma carburised and then GiC coating deposited

the samples were coded according to their treatment conditions as shown in Table 2.

2.2. Microstructure characterisation

A LECO GDS-750 QDP glow discharge spectrometer (GDS) was used to probe the chemical composition depth distribution through surface treated layer. The microstructures and chemical composition of AR, PC, GiC-AR and GiC-PC samples were studied by JEOL 7000 scanning electron microscope (SEM) with EDX accessory. A Philips X'Pert diffractometer with Cu-Kα radiation was employed to obtain X-ray diffraction charts of the samples. The scanning angle was from 20° to 100° at a scan step of 0.02° with a measuring time of 1 s per step. An Ambios XP-200 Stylus Profilers was used to profile the sliding wear tracks and surface roughness. Cross-sectional TEM sample was prepared by focused ion beam technique and the layer structure was examined using a JEOL 2100 LaB_6 Emission TEM.

2.3. Mechanical and corrosion property evaluation

A Nano Test 600 machine was used to probe the nano-hardness and reduced modulus of sample surfaces under a peak load of 25 mN for a dwell time of 10 s.

The static load bearing capacity of the surface treated samples was assessed by measuring hardness using a Mitutoyo hardness machine under a serial of loads from 25 g to 1000 g. The kinetic load bearing capacity of GiC-AR and GiC-PC samples under both normal and tangential forces was examined using a Teer ST 3001 friction-monitored scratch tester. A stationary Rockwell C spherical cone stylus was drawn across the moving sample surface under a linearly increased load at a loading rate of 100.0 N/min from 10.0 N to 60.0 N. The moving speed of sample surfaces was 10 mm/min.

A friction-monitored reciprocating TE 79 Multi-Axis Tribometer was used for both friction coefficient measurement and reciprocating wear test at room temperature in air without lubrication. In order to assess the surface friction coefficient, relatively low load and low frequency were used. While relatively high load and frequency were used to accelerate wear process to produce comparable wear tracks for reciprocating wear test. During friction coefficient measurements, a constant low load of 3.92 N was applied on a 8 mm diameter WC/Co ball sliding against moving samples at a frequency of 0.25 Hz for a stroke length of 4 mm. For reciprocating wear test, high load of 9.80 N and frequency of 1.00 Hz were applied to the same counterpart at a stroke length of 10 mm and the total sliding length was 50 m. The wear volume was obtained by integrating the cross-sectional area of the wear track determined by a profilometer and then multiplying the length of track. The wear factor was calculated by dividing the wear volume by the sliding length and the load.

Corrosion tests were performed electrochemically at room temperature in a flat cell with a three-electrode set-up in Ringer's solution. An Ag/AgCl electrode served as the reference electrode, a platinum wire worked as the auxiliary electrode and sample served as the working electrode. Sample was placed against a Teflon ring at one end of the flat cell, leaving 1 cm^2 area exposed to the ringer's solution. The test control, data collecting and processing were controlled by Solartron 1280 electrochemical measurement system

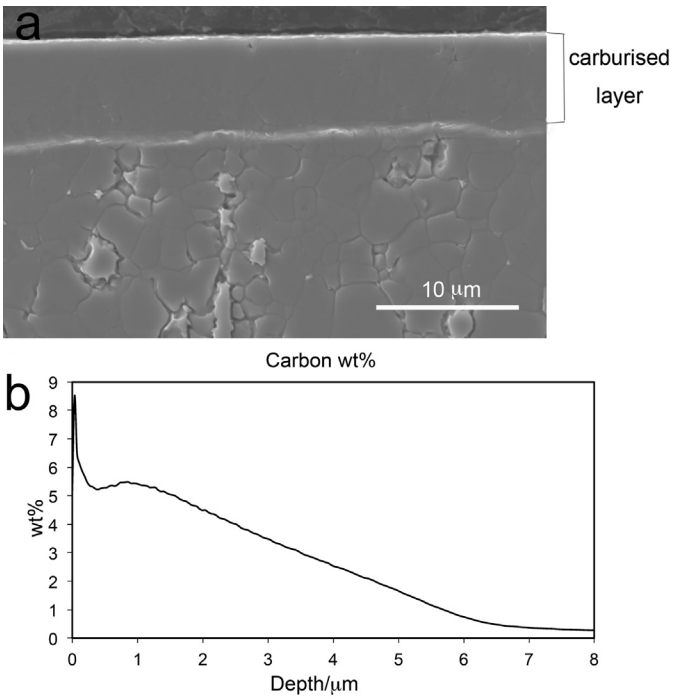

Fig. 2. (a) Cross-sectional SEM microstructure and (b) GDS carbon depth profile of the PC sample.

with Corrware software. Potential scanned from −0.250 to +1.300 V vs. OCP at a scanning rate of 1 mV/s.

3. Results

3.1. Microstructure and chemical composition

A cross-sectional SEM microstructure of the PC sample is shown in Fig. 2a, revealing a surface layer with a thickness of about 6 μm. The carburised layer exhibited better corrosion resistance than the substrate since the carburised layer was not etched while the substrate was fully etched by the same etchant used.

GDS depth profiles of the PC sample in Fig. 2b demonstrated that carbon diffused into the surface of the Co–Cr–Mo sample during the plasma carburising process and peaked at the outmost surface (5–6 wt%). As the distance from the surface increased, the concentration of carbon decreased to a substrate value at the depth of 6 μm, in good agreement with SEM observation (Fig. 2a) of the carburised case.

Fig. 3 shows surface morphology and cross-section microstructure of GiC coating on PC (GiC-PC) sample, revealing a cauliflower-like surface feature (Fig. 3a) and a very dense fine columnar coating layer structure with a thickness of about 2 μm. No sign of cracks within layer or adhesive failure between the interface of coating and substrate was observed (Fig. 3b). Surface roughness (R_a) values of all experimental samples are shown in Fig. 4. It reveals that plasma carburising increased surface R_a from 13.2 nm to 40.4 nm, which resulted in the increased R_a of GiC-PC sample.

3.2. Phase identification

The XRD patterns of AR, PC and GiC-PC samples are shown in Fig. 5. It can be seen that the untreated sample possesses two phases of α-FCC and ε-HCP with strong FCC phase constitution as evidenced by strong intensities of α(1 1 1) and α(2 0 0) peaks. The PC and GiC-PC samples showed a similar XRD peak at 2θ 47.4° which can be indexed to S-phase (2 0 0). The *d*-spacing of S(2 0 0)

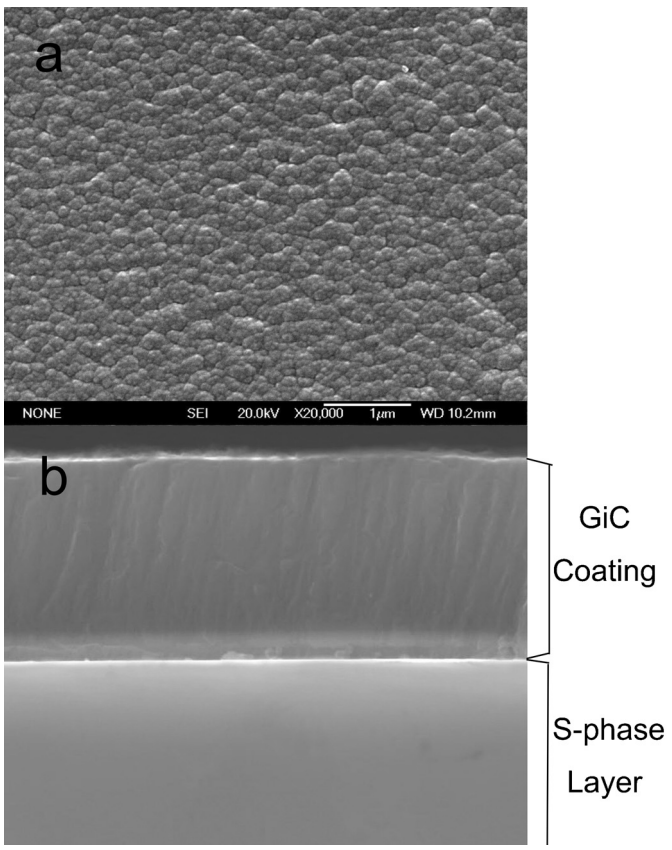

Fig. 3. SEM images of the GiC-PC sample: (a) surface morphology and (b) cross-sectional microstructure.

was 0.191 nm, which is significantly larger than that of the α(2 0 0) (0.179 nm) implying the supersaturation of carbon in S-phase. The lattice parameter of the S-phase was calculated to be $a = 0.382$ nm. A strong peak at 2θ 44.5° in the XRD pattern from GiC-PC samples (Fig. 5) can be indexed to Cr(1 1 0), since Cr was deposited as the interface layer between the top GiC coating and the substrate. No peaks other than (1 1 0) were detected, indicating a preferred orientation of (1 1 0) parallel to the coating surface. XRD patterns of S(1 1 1) and ε(1 0 1) overlaps between the angles ranging from 40.0° to 45.0°, making it difficult, if not impossible, to index them.

Fig. 6 shows cross-sectional TEM microstructures and corresponding SAD patterns of a GiC coating on carburised Co–Cr–Mo alloy. It can be seen from Fig. 6a and c that after plasma carburising a carbon diffusion layer was formed on the top of the Co–Cr–Mo

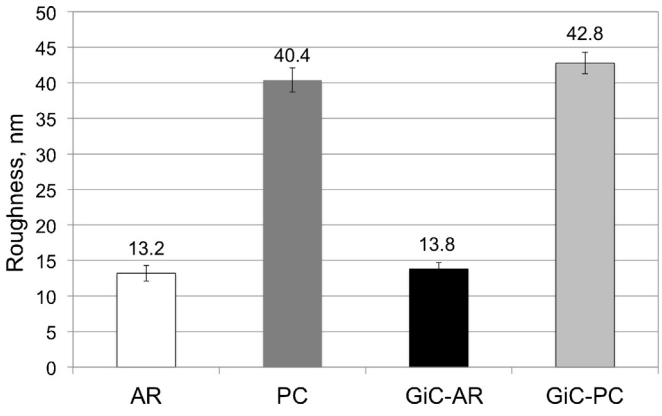

Fig. 4. Surface roughness of AR, PC, GiC-AR and GiC-PC samples.

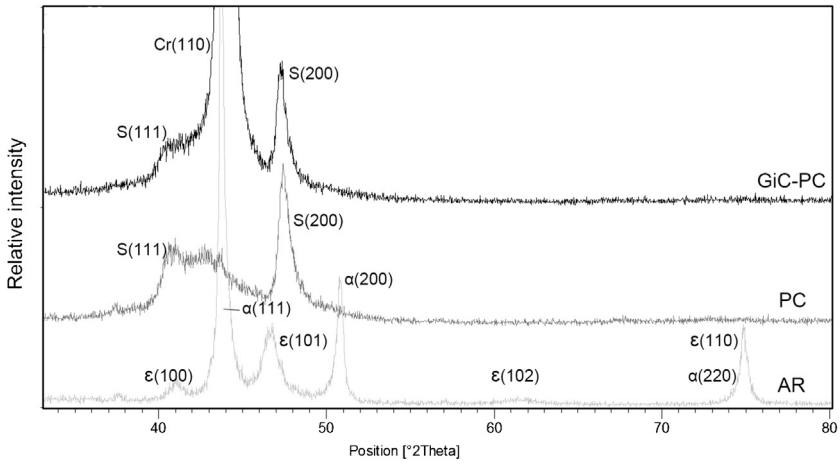

Fig. 5. XRD patterns of AR, PC and GiC-PC samples.

sample as evidenced by presenting original equal-axed grains with an α-fcc structured phase (Fig. 6c). Detailed microstructure observations along the interface between the plasma carburised surface and the GiC coating (Fig. 6b) revealed a thin (40 nm) amorphous layer at the outmost of the PC case, which was the deposition layer formed during plasma carburising. No pores and cracks could be found at the interface between the coating and the PC case, indicating a good bonding of the top GiC coating to PC case. SAD pattern (Fig. 6d) from Cr interface layer showed discrete Cr rings with strong diffraction spots of (1 1 0) planes parallel to the surface and EDX analysis has confirmed pure Cr content of this layer. This explains the strong (1 1 0) peak presented in XRD pattern of GiC-PC sample (Fig. 5).

SAD pattern (Fig. 6e) from GiC coating layer exhibits halo rings, indicating amorphous feature of the layer, as can be seen in Fig. 6b). A transition layer, evidenced by the dark gradually change contrast between the Cr layer and the GiC layer, was observed, where Cr was gradually reduced until the ratio of Cr/C in the top GiC coating.

3.3. Nanoindentation results

Fig. 7 summarises the nanoindentation results of hardness (H) and reduced modulus (Er) for AR, PC and GiC-PC samples. It can be seen that the AR sample possessed the lowest surface hardness of 6.91 GPa, the plasma carburised sample exhibited the highest surface hardness of 14.80 GPa and the GiC-PC had a hardness of 10.78 GPa. The trends are opposite for the reduced modulus with the lowest Er is for the GiC coating and the highest Er for the AR sample. The PC sample showed only slightly reduced the Er when compared with that of the AR sample.

The hardness-to-reduced modulus ratio (H/Er) is a measure of the elastic deformation capacity. The data in Fig. 7 indicate that the GiC coating has the highest H/Er ratio value.

3.4. Load-bearing capacity

Fig. 8 shows surface microhardness of GiC coating on AR and PC samples under different applied loads. It can be seen that

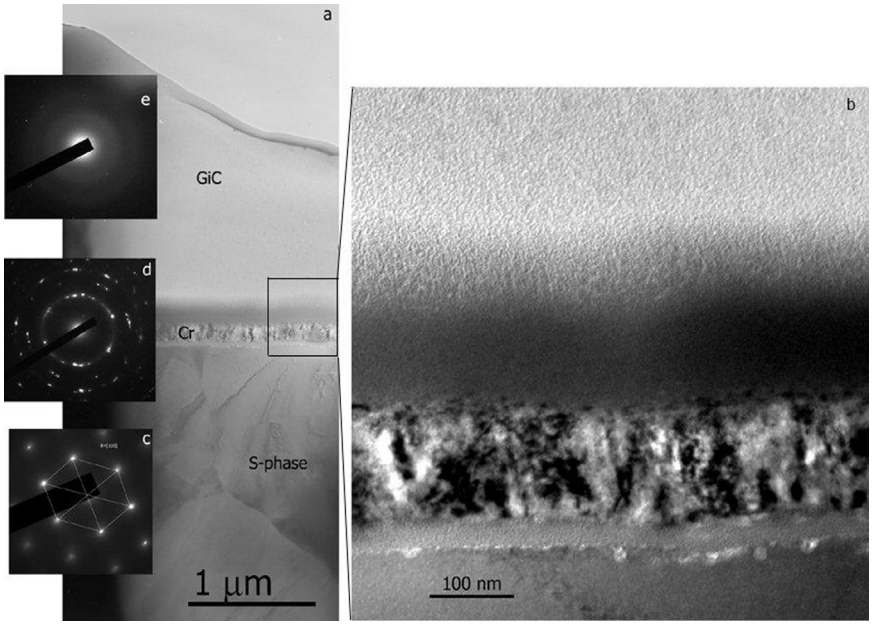

Fig. 6. Cross-section TEM microstructures of (a) layer structure of GiC coating on carburised Co–Cr–Mo substrate and (b) enlarged interface layer; SAD patterns from different areas as denoted: (c) S-phase layer, (d) Cr interface layer and (e) GiC coating.

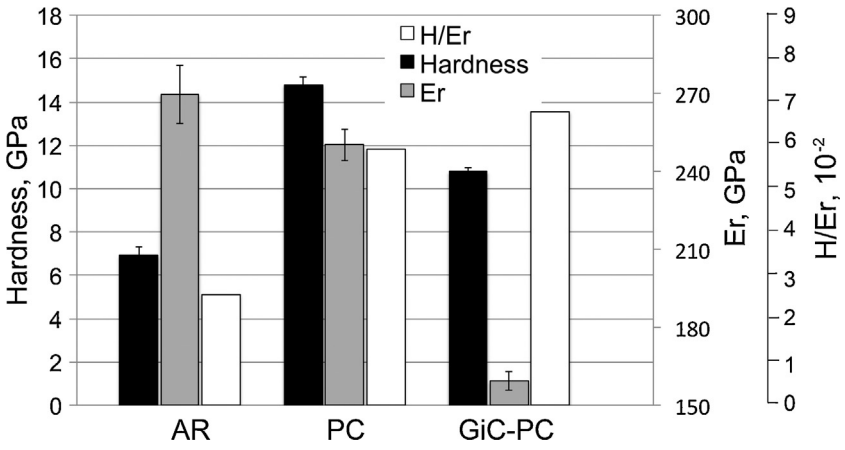

Fig. 7. Nanoindentation results of AR, GiC-AR and GiC-PC samples.

the surface hardness of GiC-AR sample reduced significantly with increasing the load, while for GiC-PC sample the surface hardness was maintained above 1000HV until a 500 g load was applied and even under the maximum load of 1000 g, its hardness is still around 700HV. The slightly higher hardness measured under 50 g and 100 g than under 25 g could be attributed to the PC subsurface, which has a higher hardness than the top GiC.

SEM observation at the indents produced under different load revealed that circumferential cracks were found within the indents when the applied load reached 50 g or above for the single coated GiC-AR sample (Fig. 9a), which is coincidently the dramatical micro-hardness decrease from 1130HV to 780HV (Fig. 8). Therefore, the loading bearing capacity of the GiC-AR sample is less than 50 g.

By contrast, for the GiC-PC duplex treated sample, no crack can be detected until 200 g, at which the surface micro-hardness dropped from 1400HV to around 1000HV (Fig. 8). Clearly, the duplex surface system can significantly enhance the load-bearing capacity of Co–Cr–Mo alloy because of the strong mechanical support from the plasma carbusing-induced S-phase case.

Fig. 10 depicts the scratch behaviour of these surface systems. For GiC-AR sample, the friction force increased gradually with the applied normal load from 10.0 N to 47.2 N (Fig. 10a). However, the SEM micrograph in Fig. 10c showed fish-bone like cracks approaching the centre of scratch groove and small cracks along the edge of the groove at the very beginning stage of scratching. As the load increased to about 24.0 N, a few chips were observed along the edge as seen in Fig. 10d. When the applied load reached 37.1 N, the first buckle cracking was observed (Fig. 10e). The density of chips increased and the fish-bone cracks evolved into net cracks within the scratch groove when further increasing the applied load. Finally, the applied load reached the critical load at 47.2 N as indicated by the sharp increase in friction force (Fig. 10a) and continuous spallation of coating was observed (Fig. 10f).

For GiC-PC sample, the friction force smoothly increased with the applied normal load and no sudden increase in friction force

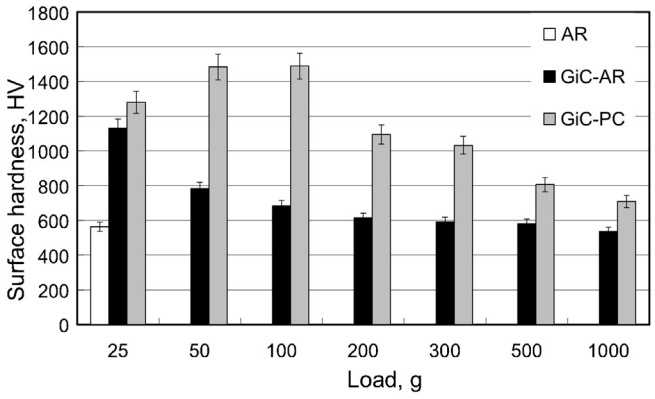

Fig. 8. Microhardness of AR, GiC-AR and GiC-PC samples under different loads.

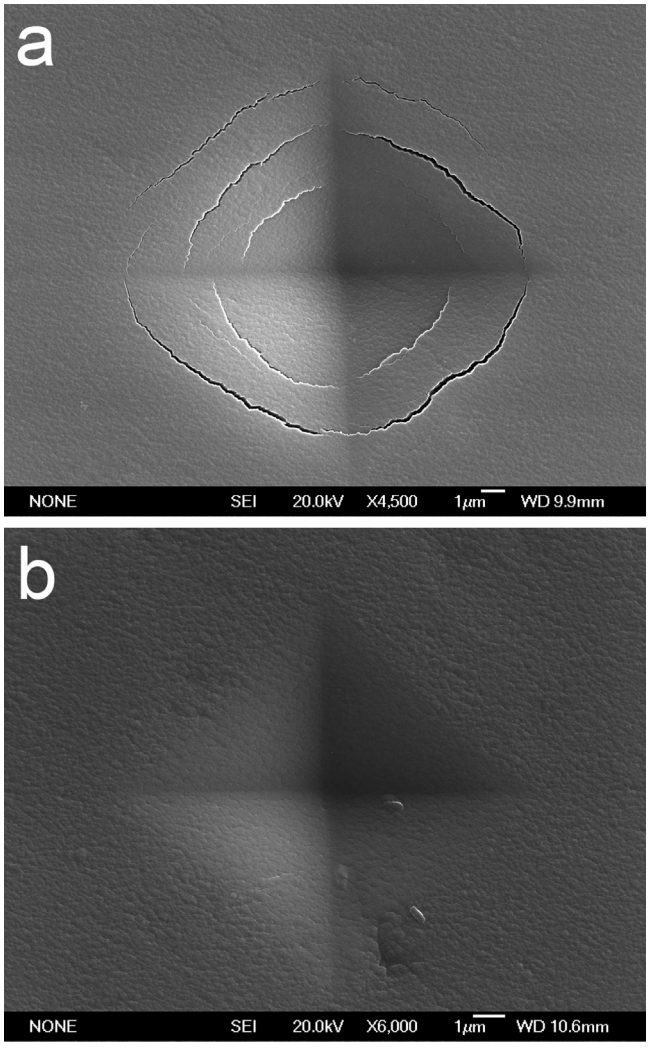

Fig. 9. SEM images of the indentations at a load of 100 g of (a) the GiC-AR sample and (b) the GiC-PC sample.

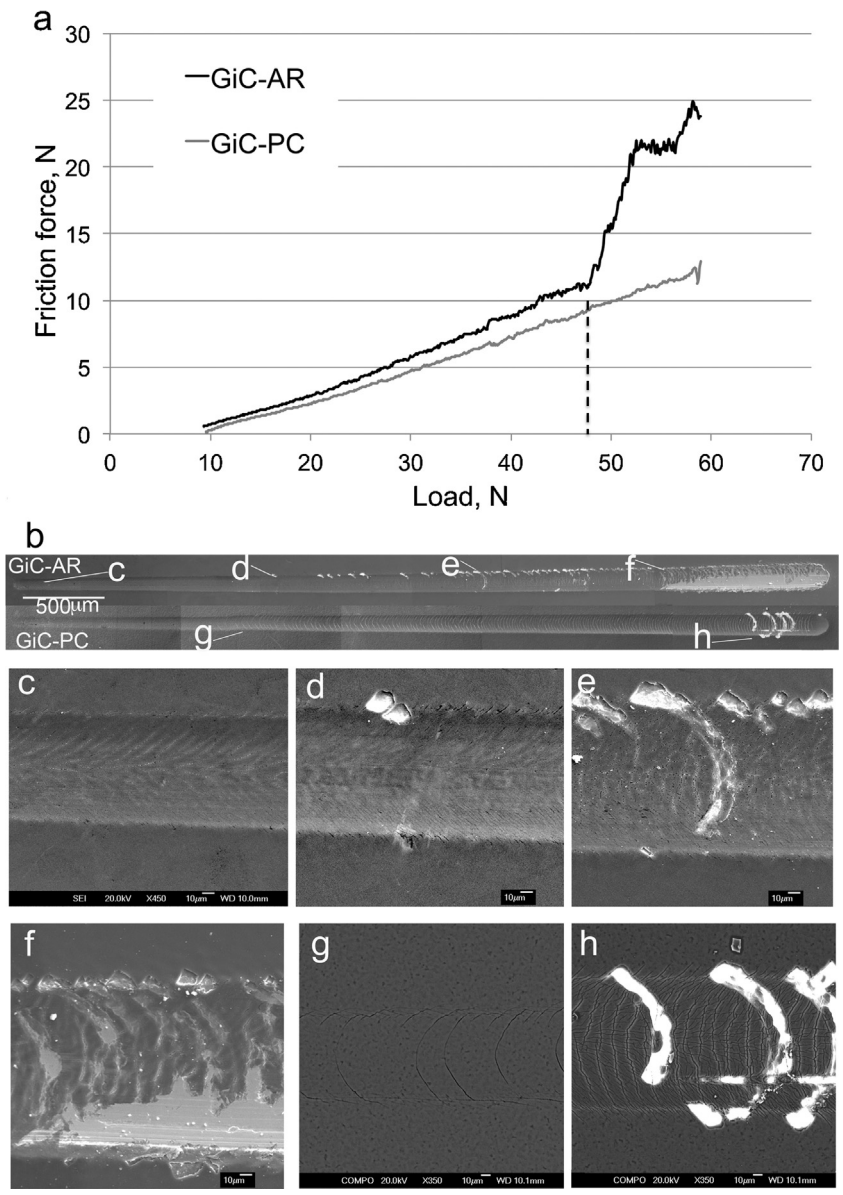

Fig. 10. (a) Friction force against scratch load and observation on scratch grooves of the GiC-AR and GiC-PC samples: (b) full versions of two scratch grooves, (c)–(f) detailed secondary electron images of the GiC-AR sample and (g)–(h) detailed back-scattered electron images of the GiC-PC sample.

can be found (Fig. 10a). However, post-scratch SEM observations revealed that tensile cracks (Fig. 10g) started to initiate at a normal load of 23.5 N as evidenced by semicircular arc features parallel to the trailing edge of the scratch stylus. The GiC coating was adhered to the carburised subsurface. When increasing the normal load to 54.8 N, buckling failure (Fig. 10h) parallel to the leading edge of the scratch stylus occurred. It is clear from Fig. 10 that duplex treated coating system exhibited much better load bearing capacity compared to single coated system.

3.5. Friction and wear

Fig. 11 compares the friction coefficient of AR, PC and GiC-AR samples measured at a low load and at a slow speed. Plasma carburised surface showed the highest friction coefficient of 0.348. Although the average roughness of GiC-PC is higher than that of GiC-AR (Fig. 4), the GiC coatings on both as-received and carburised substrate possessed similar low friction coefficient of about 0.08, indicating little effect of roughness on friction coefficient.

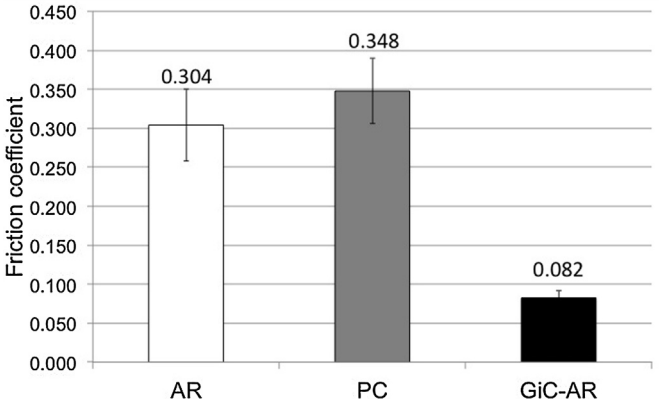

Fig. 11. Average friction coefficient of the AR and treated sample surfaces (reciprocating test, 3.92 N, WC–Co ball, 1 mm/s speed).

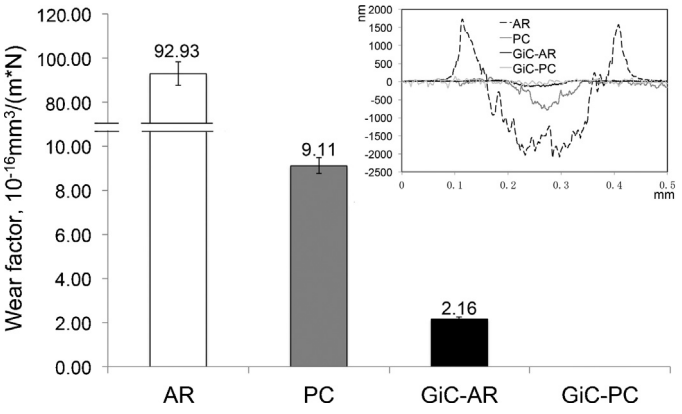

Fig. 12. Wear factor of AR and treated samples tested in air (unlubricated) at a stroke length of 10 mm at a speed of 10 mm/s against a WC/Co ball and typical cross-sectional morphologies of wear tracks.

Preliminary reciprocation sliding wear teats were conducted in air (dry wear) and the results of wear factor and typical cross-sectional wear scars are summarised in Fig. 12. It can be seen that all the surface engineered samples exhibited considerably reduced wear compared to the untreated one. The wear factor decreased from 9.29×10^{-15} mm^3 N^{-1} m^{-1} for the untreated sample to 9.10×10^{-16} mm^3 N^{-1} m^{-1} for the plasma carburised sample, representing a reduction more than 10 times. The GiC-AR samples had an even lower wear factor (2.16×10^{-16} mm^3 N^{-1} m^{-1}) than that for the PC samples. The wear track of the GiC-PC sample was not measurable under the conditions used.

The wear tracks on four types of samples were examined by SEM and EDX. The AR sample was suffered from a severe abrasive wear with many parallel abrasion marks (Fig. 13a). The plasma carburising treated sample displayed different morphologies of wear track and wear debris (Fig. 12b). Most areas of the wear track were covered by dark debris with a high content of oxygen determined by EDX. Some very fine bright particles were observed and EDX analyses revealed a high content of W, C and Co, indicating transfer of WC/Co from the counterpart ball. This suggests that oxidation wear dominated the wear process of the PC treated samples.

The wear track formed in the GiC-AR sample showed some grooves parallel to the sliding direction (Fig. 12c). Most probably, these parallel wear marks were produced by the hard asperities on the WC/Co ball with the similar damage mechanism observed during the scratch of the GiC-AR surface system (Fig. 10). The wear track formed in the duplex treated samples (Fig. 12d) was very shallow and superficial, showing excellent wear resistance under current sliding condition. This could be attributed to the very high load-bearing capacity conferred by the PC treated subsurface.

3.6. Corrosion

The corrosion behaviour of AR, PC, GiC-AR and GiC-PC samples was investigated by anodic polarisation test in terms of corrosion potential and anodic current in Ringer's solution. It can be seen from the anodic polarisation curve in Fig. 14 that all the surface engineered samples exhibited anodic shift in the corrosion potentials compared to the as-received AR sample, revealing an improvement in corrosion resistance due to either S-phase or GiC coating. The corrosion potential of GiC-AR and GiC-PC was comparable at −0.141 and −0.128 V vs. Ag/AgCl, respectively, which is nobler than that of the PC sample (−0.161 V vs. Ag/AgCl). The PC sample also showed a higher anodic current density under potential below 0.466 V vs. Ag/AgCl than the AR sample, but the opposite occurred when further increasing the potential. GiC-AR and GiC-PC samples revealed very similar corrosion behaviour under current electrochemical

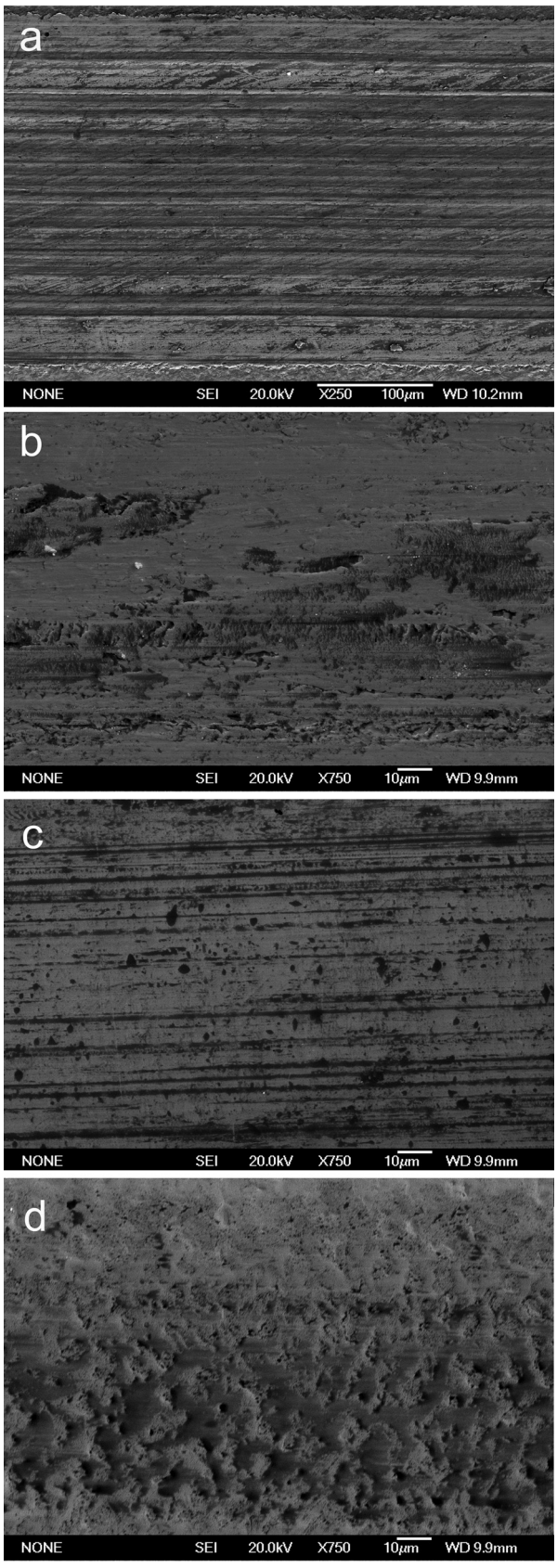

Fig. 13. SEM observation on wear tracks of (a) AR, (b) PC, (c) GiC-AR and (d) GiC-PC samples.

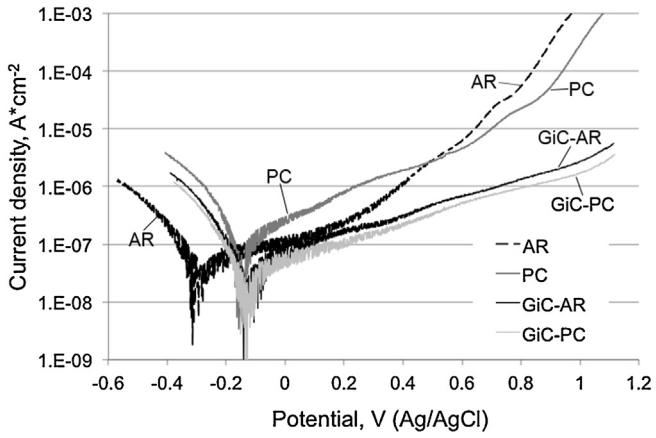

Fig. 14. Anodic polarisation curves of the AR and treated samples.

corrosion testing conditions. Their current densities are constantly lower than those of AR and PC samples due to the excellent chemical inertness and corrosion resistance of the surface GiC coating.

4. Discussion

4.1. Effect of duplex surface system on load bearing capacity

From the results above, it is clear that the duplex treated GiC-PC sample exhibited a much higher load bearing capacity under both static and kinetic conditions and improved wear resistance than the single coated GiC-AR sample.

It has been reported that a hard thin TiN coating on soft steel substrate system is prone to collapse due to plastic deformation of substrate, i.e. so-called 'thin-ice' effect [18]. For the single coated GiC-AR sample, the substrate is not strong enough to provide a sufficient mechanical support for the thin GiC coating under a high contact load. This caused coating bending and a tensile stress concentration in the contact area (especially at the edge of the contact area), thus causing the initiation of cracks in the coating when the tensile stress exceeded the coating strength. This is demonstrated by the ring cracks shown in Fig. 9a formed during static load bearing capacity tests by indentation and cracks within and along the edge of scratch grooves shown in Fig. 10b formed during dynamic load bearing capacity tests by scratching.

For the new duplex surface system, the Co–Cr–Mo substrate has been effectively hardened by plasma carburising prior to the GiC coating through the formation of carbon supersaturated super hard S-phase, so that the GiC coating can be sufficiently supported by the hardened S-phase case under a higher load and the initiation of cracks can be postponed. Consequently, the significantly improved load bearing capacity of GiC coating on carburised layer for the GiC-PC duplex system can be mainly attributed to the stronger mechanical support from very hard (14.8 GPa) S-phase layer as opposed to soft (6.91 GPa) as-received Co–Cr–Mo alloy. The reduced mismatch in mechanical properties such as hardness and H/Er between a coating and a substrate can cut down asynchronous elastic recovery of the substrate and the coating after unloading, thus minimising the occurrence of small chippings during scratch tests and cracking during indentation tests [19].

The much-improved load bearing capacity has contributed to the superior wear resistance of the duplex surface system to the single coating sample. This is mainly because the hard asperities on the WC/Co ball will penetrate into and scratch the GiC coated surface during reciprocating sliding wear tests. Alike indenter used in indentation and scratch, such hard asperities will cause stress concentration, deformation and damage of GiC coating if the subsurface cannot withstand the loading and support the surface thin coating. This is supported by closely examining the wear morphologies of single coated GiC-AR sample. Some craters and short cracks were observed in the wear track of single coated GiC-AR surface (Fig. 13c), which are caused by the hard WC asperities most probably via the similar mechanisms to indentation cracking and scratch bulking/cracking. Such greatly improved load bearing capacity and wear resistance could have scope for prolonging the life-span of metal-on-metal replacements and further work (such as wear tests in Ringer's solution with Co–Cr–Mo against Co–Cr–Mo) is needed to release the potential.

4.2. Corrosion behaviour of duplex surface system

It has been widely reported that carbon-based coatings (such as GiC coating) possess excellent corrosion resistance due to their chemical inertness [11] and can serve as an isolating film [20]. However, it has also been noticed that corrosion solution could penetrate through such defects as pinholes in thin coating to establish a galvanic cell normally with the inert coating as the cathode and the active substrate as the anode; spallation of coating would occur surrounding the pinholes due to the corrosion of the substrate and the formation of low-density and large volume corrosion products at the coating/substrate interface [8,11].

As reported in Section 3.6, the S-phase case formed during low-temperature carburising can effectively increase corrosion potential of Co–Cr–Mo alloy (Fig. 14). Hence, it is reasonable to expect that the S-phase layer beneath the GiC coating could reduce the tendency of pinhole-related galvanic corrosion due to the reduced potential difference between the GiC coating and the substrate.

However, the results in this study showed that the single coated GiC-AR and the duplex treated GiC-PC exhibited similar corrosion behaviour in terms of the corrosion potential and anodic current. The possible reason for this similarity would be the multi-layer structure of the GiC coating. As can be seen from Fig. 6, the GiC coating contains three sublayers: a columnar pure Cr adhesive layer directly deposited on the substrate followed by a Cr/C transition layer and finished by an outmost amorphous layer. Therefore, it is expected that the number of through-coating pinholes could be reduced by the multi-layer structure due to the low possibility of aligning the pinholes in different sublayers. Fig. 15 schematically shows pinholes in GiC coatings on as-received Co–Cr–Mo alloy and on S-phase layer. It should also be pointed out that, the duplex treated GiC-PC system outperformed although marginally the single coated GiC-AR in terms of slightly higher corrosion potential and consistently lower corrosion current. This can only be attributed to the different substrate below the GiC coating because the GiC coating for both the GiC-AR and GiC-PC systems were deposited in the same PVD chamber. As schematically shown in Fig. 15, the interface Cr layer could retard but difficult (if not possible) to stop the penetration of corrosive electrolyte to research the Co–Cr–Mo substrate. Therefore, the formation of S-phase beneath the GiC coating should reduce the severity of galvanic corrosion due to the reduced corrosion potential difference between the GiC coating and S-phase than between the GiC and untreated Co–Cr–Mo.

This benefit effect is expected to significantly increase if the duplex system is applied to metal-on-metal joint prostheses. This is because there is no extra pressure in the liquid electrolyte during laboratory electrochemical corrosion tests in open air. However, it is known that depending on the sliding speed, the radius of the femoral head, clearance and surface roughness of the components, metal-on-metal hip joints can work in three different lubrication regions: boundary, mixed lubrication and full fluid lubrication or elastohydrodynamic lubrication (EHL) [21,22]. High pressure is needed for the formation of EHL, which will force the lubricant

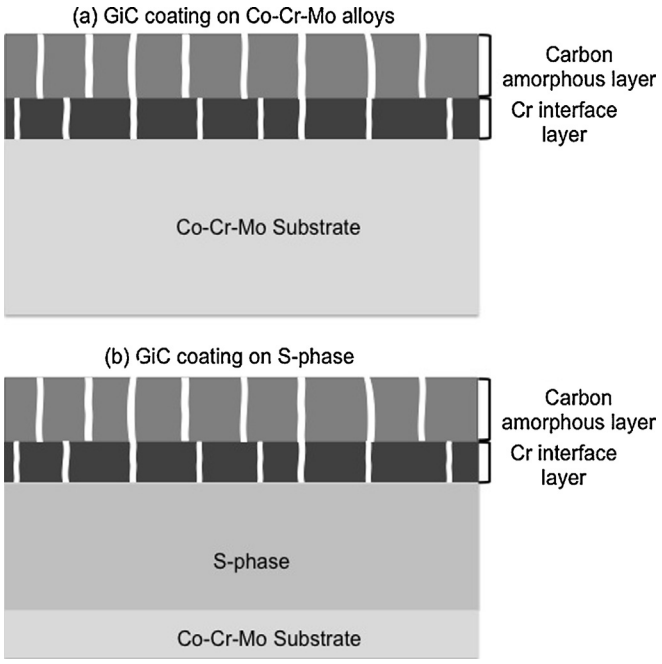

Fig. 15. Schematic of pinholes in GiC coatings on as-received and S-phased Co–Cr–Mo alloy surfaces.

or corrosive body fluid penetrate through the pinholes in GiC coating to reach the substrate, thus leading to fast galvanic corrosion. Hence, the S-phase sublayer beneath the GiC coating is expected to improve the performance of GiC coating on MOM tribopair in vivo. Future work has been planned to prove this hypothesis.

5. Conclusions

1. A duplex surface system has been successfully developed and applied to ASTM F1537 Co–Cr–Mo alloy by combining a low friction PVD GiC coating with plasma carburising induced S-phase layer.
2. The friction coefficient of S-phase formed in Co–Cr–Mo alloy by low temperature plasma carburising treatment can be reduced from 0.348 to 0.082 by duplex treatment with a top GiC coating.
3. The load bearing capacity (LBC) of GiC coating on Co–Cr–Mo alloy can be effectively enhanced by duplex treatment through hardening the Co–Cr–Mo substrate: the static LBC measured by indentation has increased from 50 g to 200 g; the dynamic LBC measured by scratching in terms of the 1st and 2nd critical loads increased from about 10.0 and 47.2 N, respectively, to 23.5 and >60.0 N.
4. The wear factor of single coated GiC on Co–Cr–Mo alloy has been reduced dramatically from 2.16×10^{-16} mm^3 N^{-1} m^{-1} to nearly 0 under the current testing conditions by hardening the Co–Cr–Mo substrate to form the GiC-PC duplex system.
5. The GiC-PC duplex system can significantly increase the corrosion potential and reduce the anodic current density of Co–Cr–Mo alloy mainly due to the highly corrosion-resistance GiC coating in conjunction with an S-phase substrate layer with improved corrosion potential as compared to untreated Co–Cr–Mo alloy.

Acknowledgements

The authors would like to acknowledge the financial support from EPSRC (EP/J018252/1) and thank Teer Coatings Ltd for the provision of GiC coatings for this research.

References

[1] S. Virtanen, I. Milosev, E. Gomez-Barrena, R. Trebse, J. Salo, Y.T. Konttinen, Special modes of corrosion under physiological and simulated physiological conditions, Acta Biomaterialia 4 (2008) 468–476.
[2] J. Gallagher, Metal-on-metal hip replacements 'high failure rate', BBC News (2012) [cited 2012 13 March]. Available from: http://www.bbc.co.uk/news/health-17337993
[3] H. Dong, S-phase surface engineering of Fe–Cr, Co–Cr and Ni–Cr alloys, International Materials Reviews 55 (2010) 65–98.
[4] T. Bell, H., Dong, C.X. Li, Plasma surface treatment of Co–Cr biomaterial, European Patent EP 1 499 755B1 (21 May 2008).
[5] X.Y. Li, N. Habibi, T. Bell, H. Dong, Microstructural characterisation of a plasma carburised low carbon Co–Cr alloy, Surface Engineering 23 (2007) 45–51.
[6] W. Wu, X. Li, J. Chen, H. Dong, Design and characterisation of an advanced duplex system based on carbon S-phase case and GiC coatings for 316LVM austenitic stainless steel, Surface and Coatings Technology 203 (2009) 1273–1280.
[7] G. Bergmann, F. Graichen, A. Rohlmann, N. Verdonschot, G.H. van Lenthe, Frictional heating of total hip implants. Part 1: measurements in patients, Journal of Biomechanics 34 (2001) 421–428.
[8] H. Dong, Surface engineering of prosthetic bearing surfaces, in: S. Zhang (Ed.), ICSE Contributions of Surface Engineering to Modern Manufacturing and Remanufacturing, Southwest Jiaotong University Press, Chengdu, China, 2002, pp. 457–464.
[9] S.K. Field, M. Jarratt, D.G. Teer, Tribological properties of graphite-like and diamond-like carbon coatings, Tribology International 37 (2004) 949–956.
[10] G. Dearnaley, J.H. Arps, Biomedical applications of diamond-like carbon (DLC) coatings: a review, Surface and Coatings Technology 200 (2005) 2518–2524.
[11] A. Dorner-Reisel, C. Schürer, G. Irmer, E. Müller, Electrochemical corrosion behaviour of uncoated and DLC coated medical grade Co28Cr6Mo, Surface and Coatings Technology 177–178 (2004) 830–837.
[12] R.K. Roy, K.R. Lee, Biomedical applications of diamond-like carbon coatings: a review, Journal of Biomedical Materials Research Part B: Applied Biomaterials 83 (2007) 72–84.
[13] C.V. Falub, U. Müller, G. Thorwarth, M. Parlinska-Wojtan, C. Voisard, R. Hauert, In vitro studies of the adhesion of diamond-like carbon thin films on CoCrMo biomedical implant alloy, Acta Materialia 59 (2011) 4678–4689.
[14] T.J. Joyce, Examination of failed ex vivo metal-on-metal metatarsophalangeal prosthesis and comparison with theoretically determined lubrication regimes, Wear 263 (2007) 1050–1054.
[15] Z.X. Zhang, H. Dong, T. Bell, The load bearing capacity of hydrogen-free Cr-DLC coatings on deep-case oxygen hardened Ti6Al4V, Surface and Coatings Technology 200 (2006) 5237–5244.
[16] R. Hauert, An overview on the tribological behavior of diamond-like carbon in technical and medical applications, Tribology International 37 (2004) 991–1003.
[17] J. Stallard, D.G. Teer, A study of the tribological behaviour of CrN, Graphit-iC and Dymon-iC coatings under oil lubrication, Surface and Coatings Technology 188–189 (2004) 525–529.
[18] T. Bell, H. Dong, Y. Sun, Realising the potential of duplex surface engineering, Tribology International 31 (1998) 127–137.
[19] S.J. Bull, Failure modes in scratch adhesion testing, Surface and Coatings Technology 50 (1991) 25–32.
[20] A. Zeng, E. Liu, I.F. Annergren, S.N. Tan, S. Zhang, P. Hing, J. Gao, EIS capacitance diagnosis of nanoporosity effect on the corrosion protection of DLC films, Diamond and Related Materials 11 (2002) 160–168.
[21] L. Gao, F. Wang, P. Yang, Z. Jin, Effect of 3D physiological loading and motion on elastohydrodynamic lubrication of metal-on-metal total hip replacements, Medical Engineering & Physics 31 (2009) 720–729.
[22] J.L. Tipper, E. Ingham, Z.M. Jin, J. Fisher, (iv) The science of metal-on-metal articulation, Current Orthopaedics 19 (2005) 280–287.